Visual Abstract

The investigation of additive manufacturing and moldable materials to produce railway ballast grain analogs

B. Szabó, L. Pásthy, Á. Orosz, K. Tamás
Budapest University of Technology and Economics, Hungary
szabo.bence@gt3.bme.hu, pasthylaci@gmail.com
orosz.akos@gt3.bme.hu, https://orcid.org/0000-0002-4265-6900
tamas.kornel@gt3.bme.hu, https://orcid.org/0000-0001-7556-6410

ABSTRACT. The size and shape of individual grains play an important role in the mechanical behavior of granular materials such as the strength and the stability of railway ballast. The aim of this research is to investigate materials from which reproducible grains with irregular convex geometry can be produced by molding and additive manufacturing technologies in order to create replicable artificial railway ballast assemblies that can be used in experiments. Packings with controlled grain shape results more controlled investigations contrarily to using natural grains with random geometry. Specimens were made from railway ballast materials, three groups of moldable materials (materials used in the construction industry, thermosetting polymers, and certain low-strength materials) and additively manufactured polymers. Uniaxial compression and bending tests were performed on these specimens. The mechanical properties of typical railway ballast materials (basalt and andesite) were compared with the properties of artificially produced materials. Of the moldable materials, we recommend the use of polyester resin, mixed with fine-graded crushed stone aggregate or the application of ceramic powder. Furthermore, the PolyJet and Multi Jet Fusion additive manufacturing technologies produced specimens with the closest mechanical properties to basalt and andesite.

KEYWORDS. Granular materials; Railway ballast; 3D printing; Effect of shape; Uniaxial compression test; Grain breakage.

OPEN ACCESS

Citation: Szabó, B., Pásthy, L., Orosz, Á., Tamás, K., The Investigation of Additively Manufacturing and Moldable Materials to Produce Railway Ballast Grain Analogs, Frattura ed Integrità Strutturale, 60 (2022) 213-228.

Received: 29.07.2021
Accepted: 01.01.2022
Online first: 07.02.2022
Published: 01.04.2022

INTRODUCTION

The effect of size and shape of the individual particles on the mechanical properties of a granular assembly is an area of intensive research. In the case of experiments on physical assemblies of grains, the difficulty is that the geometry of the assembly and the shapes of the grains are random and vary test by test. The first solution is to characterize each assembly e.g. with the utilization of computed tomography [1]. The second solution is to control the shape of the

grains. It is difficult to create artificial grains with arbitrary geometry from typical railway ballast materials, so alternative materials and methods shall be used [2]. Experiments with carefully designed and known particle shape can also applied to calibrate or validate mechanical and breakage properties of discrete element method (DEM) models [3].
Assemblies of particles with idealized shapes are often used to model granular materials. These geometries are relatively easy to produce from a wide variety of materials. Ma and Zhao [4] used fiber reinforced plastic rods (FRP), Kodam et al. [5] used plexiglass cylinders, Maione et al. [6] used steel balls and cylindrical wood pellets, Härtl and Ooi [7] used glass spheres and paired spheres for this purpose. Wu et al. [8] performed uniaxial compression tests on Masado (decomposed grain soil), Toyoma Sand and on assemblies consisting of glass beads. Zhao et al. [9] validated DEM models by performing experiments on tetrahedral particles with different eccentricities and height ratios made of polyester.
Additive manufacturing (AM) technologies are often applied to create artificially produced granular materials. These technologies also enable to create particle geometries consisting of irregular grains. Miskin and Jaeger [10] applied PolyJet technology to produce clumped spheres from photopolymer. Athanassiadis et al. [11] created assemblies in large quantities of different convex and concave grains with a similar technique. Landauer et al. [12] also investigated the effect of shape with non-spherical grains. They also chose Selective Laser Sintering (SLS) to create particle assemblies and compare their mechanical behavior with DEM simulations.
There are many examples to the physical modelling of natural sand with additively manufactured grains. Hanaor et al. [13] produced 2 mm diameter grains by three different shape generation methods with the use of PolyJet technology. Li et al. [14] demonstrated that Stereolithography (SLA) can be used to efficiently generate large amounts of transparent soil modelling grains. Adamidis et al. [15] used additive manufacturing to reproduce natural sand in several size ranges. Various additive manufacturing technologies were examined, based on which a PolyJet technology was decided. In addition, the representativeness of the additively manufactured grain relative to the original morphology was investigated. Achmed and Martinez [16] performed experiments on steel, glass and additively manufactured spheres and their assemblies to compare their mechanical behavior with assemblies made of rounded and angular sand grains. SLA and PolyJet technology were also compared in aspects of creating granular material. The surface of the particles that were created with the SLA was found to be of better quality. Kittu et al. [17] proved that gypsum-epoxy composite and photopolymer as additively manufactured materials were suitable for the creation of sand and gravel grains and for the validation of DEM simulations. The material properties they examined were Young's modulus, Poisson's ratio, size, shape (sphericity, aspect ratio and circularity), surface roughness, and inter-particle friction angle. Kittu et al. noted that [10,13] the use of specific materials in the validation of DEM simulations to be successful, despite the fact that very little information is shared about their properties and surface characteristics. Their research revealed that the gypsum-epoxy composite and photopolymer AM materials are feasible to use in DEM validation studies, however, only spherical particles were tested in this study for ease of comparison with glass beads and steel ball bearings. As it was highlighted in the research of Kittu et al. [10,13], many papers on the validation of DEM models do not study the reason for the choice on material of the particles. Furthermore, little information was provided about properties of the chosen materials.
Based on the literature, it is possible to physically produce granular materials with additive manufacturing or molding techniques; however, there was lack of information about the potential materials for modelling railway ballast grains.
The mechanical properties of polymers differ significantly from the properties of railway ballast materials, because their failure mode is large plastic deformation. However, the advantage of the application of additive manufacturing methods relies in that a large number of small particles can be produced fast. Additive manufacturing technologies also have the potential to create an assembly of particles accurately and reproducibly based on a virtual geometry model. This model can also be the basis of a DEM simulations. Based on the deficiencies in this research field, the first aim was to compare the mechanical properties and failure mode of the investigated materials with the mechanical properties of common railway ballast materials as andesite and basalt in Hungary [24]. The second aim of this study was to investigate and test AM and molding technologies and create a process to efficiently manufacture convex polyhedral grains. Based on these measurements, it will be demonstrated which specific materials and technologies can be used to model the grains of railway ballast materials in order to create replicable artificial assemblies, that can be used in experimental shape studies.

MATERIALS AND METHODS

Material characteristics of test specimens

AM and molding technologies were applied to manufacture specimens from several materials (Tab. 1) to investigate their compression and bending properties. Uniaxial compression and three-point bending tests were performed. Cubic specimens with an edge length of 20 mm were prepared for compression tests. The dimensions of the

specimen of bending test specified in DIN 53452 was 120x15x10 mm [18]. Fig. 1 shows these specimens. A custom-designed mold was used to produce the molded specimens. Additive manufacturing technologies made it possible for specimens to be manufactured directly from their 3D geometry models. At least five compression and five bending specimens were prepared from the tested materials.

Material	Technology used to prepare the test specimen	Description of material	Notation on Fig. 1
Andesite	Cut from tiles	-	K, L
Basalt	Cut from tiles	-	M
Concrete	Molding	Baumit C20/25 premixed concrete	Q
Mortar	Molding	Screened Baumit C20 / 25 premixed concrete	R
Socket leveler	Molding	Ultraplan eco 20	P
Ceramic powder	Molding	-	T
Expanded Polystyrene (EPS) adhesive	Molding	Styrokleber EPS system adhesive	O
Clay soil	Molding	-	I
Crosslinked polyurethane resin (PUR) with aluminum trihydrate (ATH) adhesive (0, 100, 200)*	Molding	F190 Quick mold	C, D, E
Crosslinked epoxy resin	Molding	EC 141 NF/W 241	B
Crosslinked polyester resin	Molding	Synolite 0328	S
Polyester-crushed stone composite	Molding	Synolite 0328 + screended Baumit C20/25	U
Acrylonitrile-butadiene-styrene (ABS)	AM (FDM)	-	G
Polylactic acid with 60% filling (PLA)	AM (FDM)	-	F
Polylactic acid with 100% filling (TPLA)	AM (FDM)		J
Polyamide	AM (Multi Jet Fusion)	PA12	A
RGD 835	AM (PolyJet)	-	

* The number indicates the quantity of ATH adhesive in percentage.

Table 1: The materials and technologies.

Uniaxial compression and three-point bending tests

Uniaxial compression and bending tests were performed on a Zwick Z050 (serial no.: 151201/2001) universal material testing machine taking into account several recommendations of the standards for polymers ISO 604 [19] and ISO 178: 2009 [20]. For andesite and basalt specimens, the uniaxial compression tests were performed on a Zwick Z250 (serial no.: 208800/2012) universal materials testing machine. During the measurements, the software of the measuring instrument recorded the force measured by the load cell at a frequency of 50 Hz and the displacement of the pressure plate of the machine. The tests were performed at a constant speed of 5 mm/min. For most materials, the maximum pressure plate displacement was set at 5 mm and the force limit was set at 40 kN for the Z050 and 200 kN for the Z250. It was also set that if the force drops by 80% from a previous maximum value, the test will be stopped. Within a series of measurements five repetitions were made.

The three-point bending test is shown in Fig. 2. In the case of andesite and basalt, it was different from this arrangement. The support distance was also 100 mm, but the height and width of the specimens were 20 mm.

Optical measuring system based on digital image correlation technique

Digital image correlation (DIC) technique was applied to analyze the displacement, as in [21,22]. The compression tests were recorded with a Mercury Monet Video Extensometer at a sampling frequency of 10 Hz. After calibration of the camera, on the previously painted surface of the specimens with the utilization of the extensometer's software (Fig. 3) virtual point

pairs (marked as purple crosses) were defined and their relative displacement to each other (marked as green sections) were captured. The strains were calculated from the point pair that forms the middle vertical section. During the analysis, the failure mode of each specimen was also analyzed.

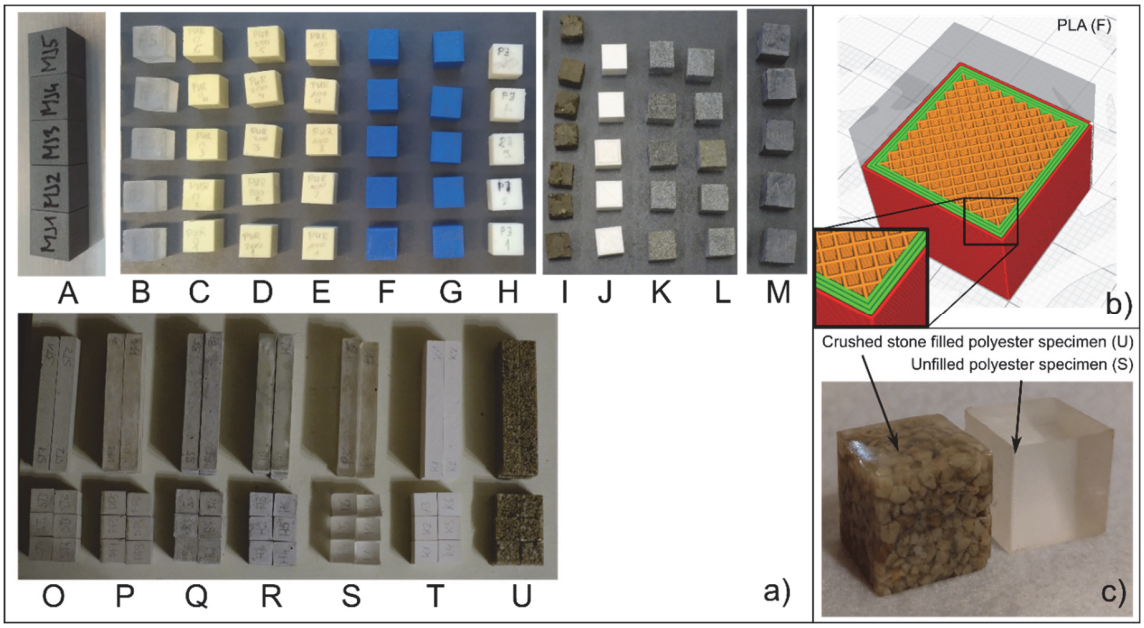

Figure 1: Specimens a) tested compression and bending specimens (The notations refer to Tab. 1.), b) grid structure of the infill density in PLA specimens (F), c) filled (U) and unfilled (S) crosslinked polyester specimens.

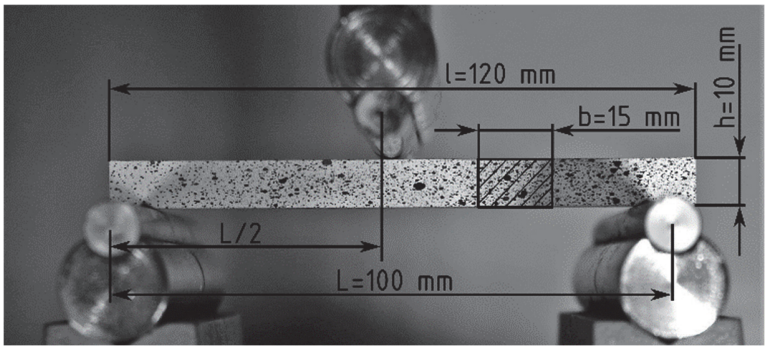

Figure 2: Arrangement of three-point bending test.

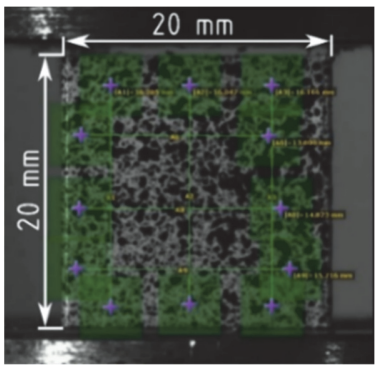

Figure 3: Virtual strain gauge on a cubic compression specimen for DIC.

Evaluation of data

Five individual tests were conducted for each material, then averaged stress-strain diagrams were computed (Figs. 5, 6, 8, 10 and 12). The stress-strain diagrams of the individual experiments were shifted horizontally along the strain axis to be able to compute the averaged curves and to eliminate the effect of specimen irregularities (e.g. non-parallel faces and surface asperities). The shift was made as follows: lines were fitted with the use of least squares fitting method on the linear section of the curves then the curves were translated horizontally so that the fitted lines intersected the origin. As the stresses and the steepnesses of the curves did not change, the shifting had no effect on the compressive and flexural strength and compressive and flexural Young's modulus, however it had an impact on compressive and flexural strain. Note that the horizontal shifting is often applied during the evaluation of compression test, as performed by e.g. Suhr and Six [23].

The applied process to produce the grain analogs

AM technologies are often used to print granular materials directly. It was demonstrated in the literature review that they can create irregular shapes, therefore they can be used to produce convex polyhedra grains as well, which was used to model ballast grains. Another solution to produce these simplified railway ballast grains in large quantities is the molding, however, there is no description in the literature on how to perform this process, therefore a novel method was developed and tested (Fig. 4). Firstly, master samples (green) are printed with preferably a high-accuracy, e.g. PolyJet AM technology and which are then used to create silicone shell molds (blue on Fig. 4). Multiple silicone molds can be created with the same master samples. Optionally, an outer mold (red on Fig. 4), can be produced as well, preferably with a low-cost, e.g. FDM AM technology to save silicone material and reduce manufacturing costs. Then, large quantities of polyhedral and angular shaped grains can be created with the silicone molds.

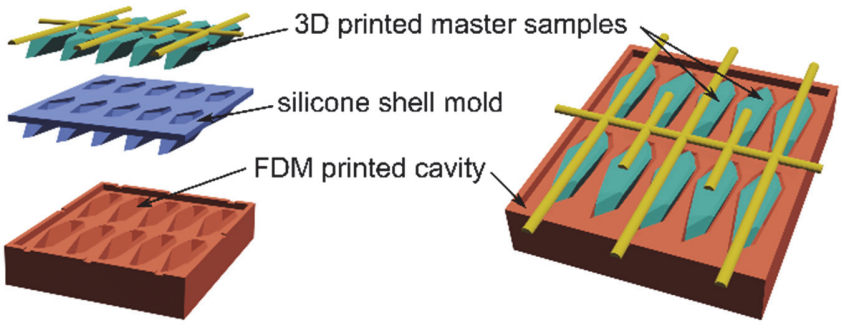

Figure 4: Creation process of a silicone mold.

RESULTS

Test results of railway ballast materials

The stress-strain diagram of the uniaxial compression tests of andesite and basalt are shown in Fig. 5. These test results were used as a reference in the evaluation of the measurement results of further investigated materials. An explosive failure of the test specimens occurred at the end of the measurement. In most cases, a single rectangular pyramid remained from the specimen after the breakage.

Test results of materials in construction industry

The stress-strain curves of the uniaxial compression tests of the materials applied in construction industry are shown in Fig. 6. Fig. 7 is showing snapshots of the crack propagation during the uniaxial compression test process.

During the uniaxial compression test of concrete (Fig. 7 a), an initial crack occurred within stress range 16.25-23.75 MPa. After the breakage, the bottom and the top of the concrete specimens remained symmetrical in the shape of a cone, while the sides fragmented. The tests were stopped at this point because the compression force dropped by 80% of the maximum measured value at this time, however, the failure did not occur explosively.

The failure process of mortar (Fig. 7 b) and socket leveler (Fig. 7 c) are discussed together because of their similarity. The Young's moduli of these two materials are very similar, though, higher values of compressive strength were obtained in the case of socket leveler. For both materials, the bottom and the top of the specimen remained in the form of a cone after

their failure. The difference is that while corner cracks appeared on the surface of the mortar from the beginning of compression, in the case of the socket leveler this was only observed for the first time in the stress range of 12.7-20.75 MPa. During the uniaxial compression tests on the specimens made from ceramic powder, initial cracks suddenly appeared in the stress range of 18.75-33.75 MPa (Fig. 7 d). Small, sudden drops in the stress appeared on each individual stress-strain curve, which is not visible on the averaged curves. The fractures appeared parallel to each other, which indicates that the failure form of the specimen was splitting. This form of failure was not shown by the other investigated materials.

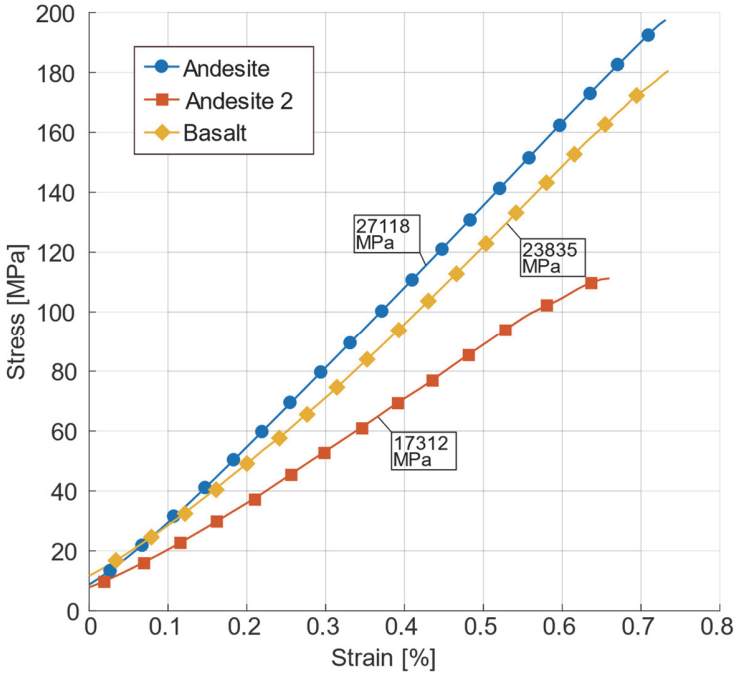

Figure 5: Averaged stress-strain diagram of compression tests on railway ballast materials (The Young's moduli are indicated).

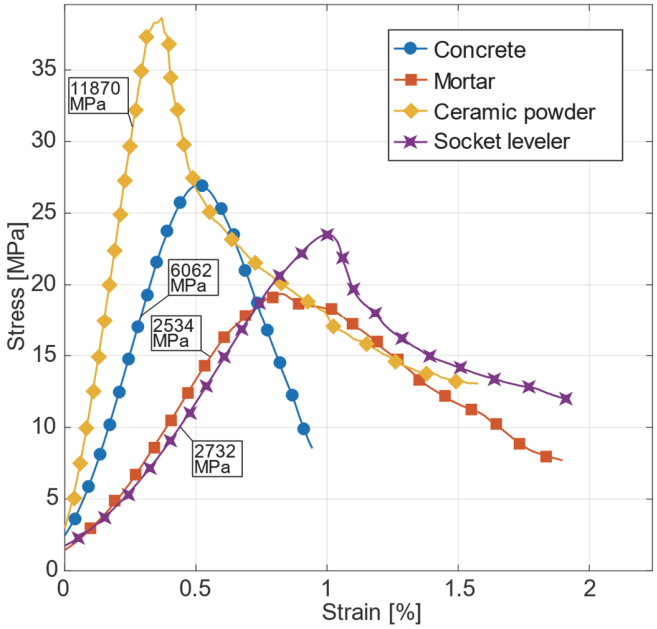

Figure 6: Averaged stress-strain diagram of compression tests on materials used in construction industry (with indicated Young's moduli).

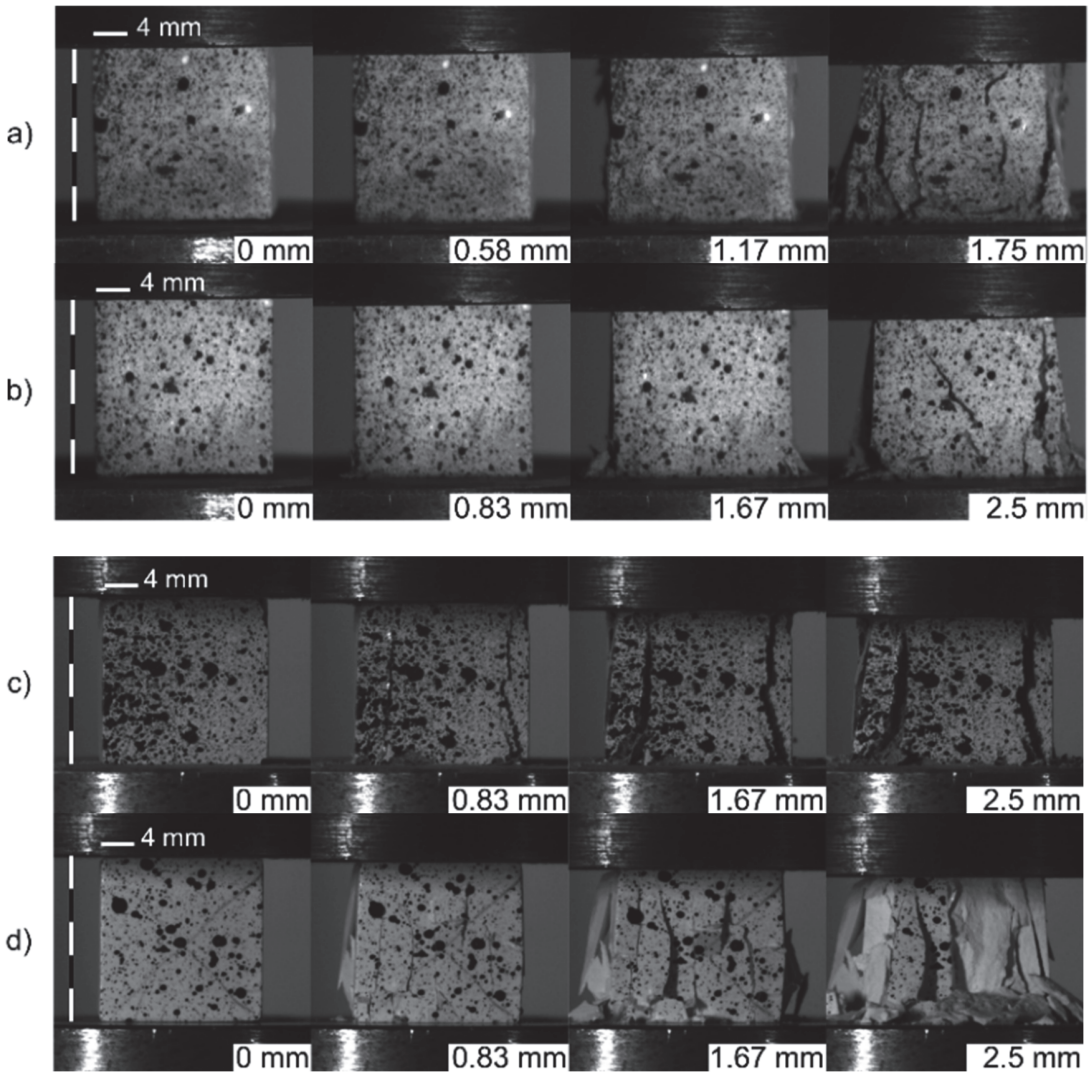

Figure 7: Failure process of construction materials, a) concrete, b) mortar, c) socket leveler, d) ceramic powder (The magnitude of vertical displacements was indicated on figures).

Test results for additively manufactured polymers

The stress-strain curves of additively manufactured materials are shown in Fig. 8. The specimens made with PolyJet technology have the highest compressive strength. Moreover, there is a long linear section at the beginning of the curve. Fig. 9 d) and e) shows the uniaxial compression tests of polymers printed with PolyJet technology. The failure modes of the PolyJet specimens were not consistent, which might be caused by the anisotropy in their material structure due to the manufacturing technology.

One face of the cubic specimens manufactured with Multi Jet Fusion technology, showed a significant difference in surface roughness. The compressive strength of the PA12 specimen manufactured with Multi Jet Fusion technology and the TPLA and ABS specimens manufactured with FDM cannot be defined, as their curves increase monotonically from the beginning over the entire measurement range. In these cases, instead of the compressive strength the strain was determined at the yield point, because the linear phase ends here. PLA specimens were prepared at 60% infill density (the volumetric percentage of the polymer) with a grid structure that has a 2 mm thickness (Fig. 1 b), because incomplete infill density is often set when the FDM is applied. As a result, its compressive strength became lower than if they were made at full infill density. Furthermore, during the failure process, protrusion or creasing could be observed in pairs on the sides of the specimens (Fig. 9 a).

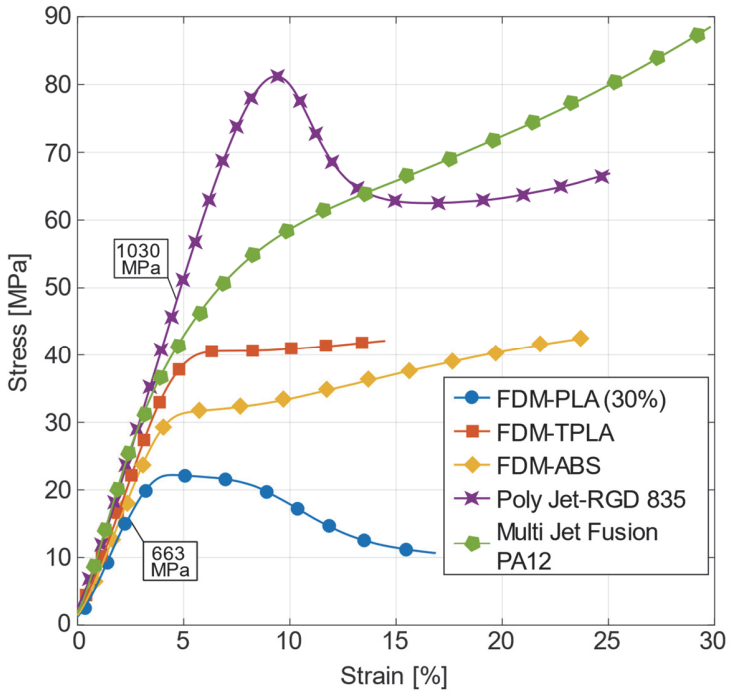

Figure 8: Averaged stress-strain diagram of compression tests on additively manufactured materials (The smallest and greatest Young's moduli are indicated).

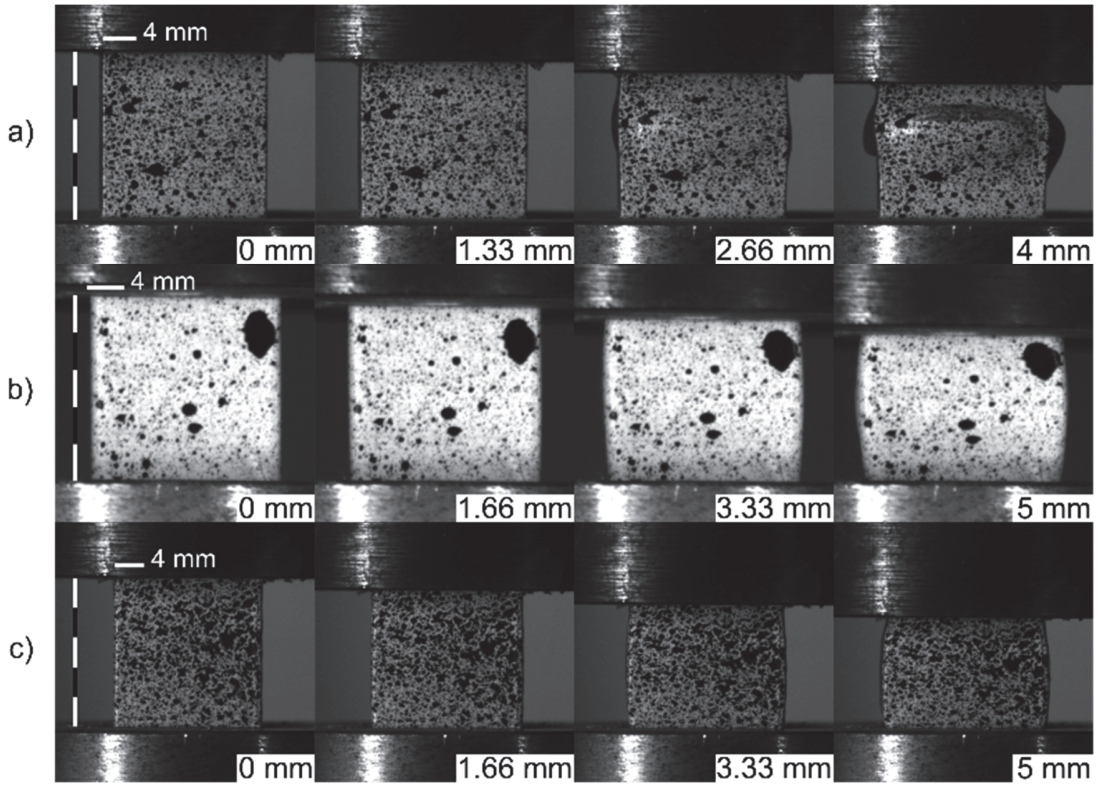

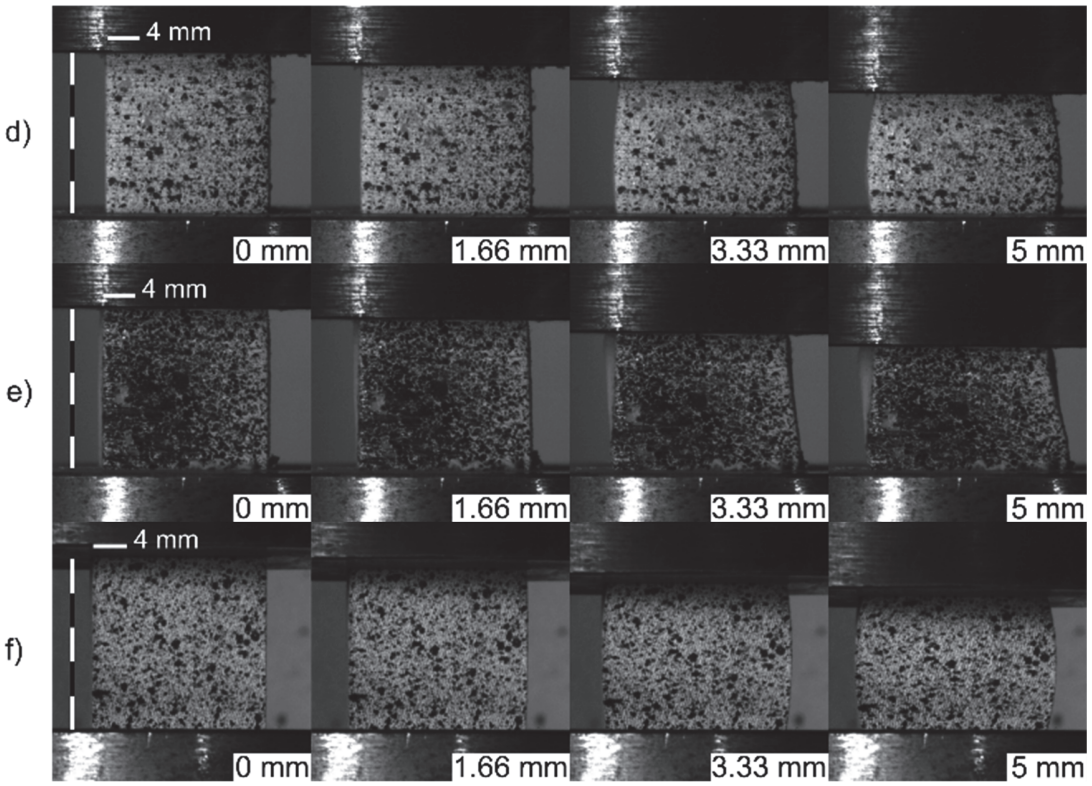

Figure 9: Failure process of additively manufactured materials a) PLA (FDM), b) TPLA (FDM), c) ABS (FDM), d) symmetric failure of PolyJet specimen, e) asymmetric failure of PolyJet specimen, f) PA12 (Multi Jet Fusion) (The magnitude of vertical displacements was indicated on figures).

Test results for molded thermosetting polymers

In the case of molded thermosetting polymers, both filled and unfilled polyester specimens (Fig. 1 c) were tested. The stress-strain curves on Fig. 10 show that the strength and stiffness of the base resins is significantly dependent on filling. This is also confirmed by the results of bending tests. In the case of bending, two of the five unfilled polyester specimens reached the deflection corresponding to 10% of the support distance at a stress of around 65 MPa. However, in the case of the other three unfilled polyester bending specimens, failure occurred at lower stress with breakage, between 50-52 MPa. In the case of three specimens the breakage occurred suddenly, and the specimens broke into several pieces, however there was no breakage in the case of the other two specimens. Filling with crushed stone reduced the average strain of the specimen at compressive failure by more than one-seventh and reduced its flexural strength by more than 50%. The failure mode was also affected by the filling of the base resin. The polyester bending specimens filled with crushed stone showed brittle breakage into two parts. In the case of the uniaxial compression tests on pure polyester specimens (Fig. 11 b), the measuring range of the material testing machine was reached before reaching the specimen's compressive strength value. However, as a result of filling with crushed stone, the failure occurred in a sudden explosion at the end of the test, (such failure is shown in Fig. 11 f), or the specimen broke into several little pieces remaining between the pressure plates. In the case of explosive failure, the bottom and the top of the specimen typically remained in the form of a cone (highlighted with lines at Fig. 11 f). It can also be observed that the adhesive bond formed between the crosslinked polyester resin and the filling grains is so strong that the fracture surfaces also pass through the crushed stones. During the uniaxial compression test, the initial crack of this material typically occurred in the stress range of 57.5-77.5 MPa.

Analyzing the failure processes of polyurethane (PUR), it can be observed that by increasing the amount of aluminum trihydrate (ATH) filler mixed into the resin, the residual deformation of the specimen did not affect. Furthermore, by increasing the amount of ATH mixed into the resin, the deformation at which cracks occurred, decreased (Fig. 11 c, d, e). The failure forms of unfilled PUR and epoxy resin specimens show similarities to the failure forms of additively manufactured specimens. Their failure is also accompanied by elastic and plastic deformation.

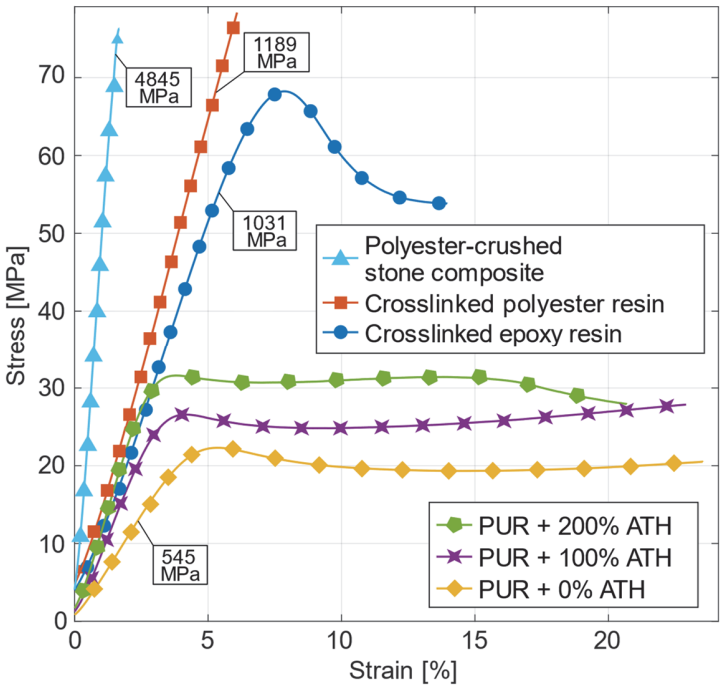

Figure 10: The stress-strain diagram of compression tests on molded thermosetting polymers (with indicated Young's moduli).

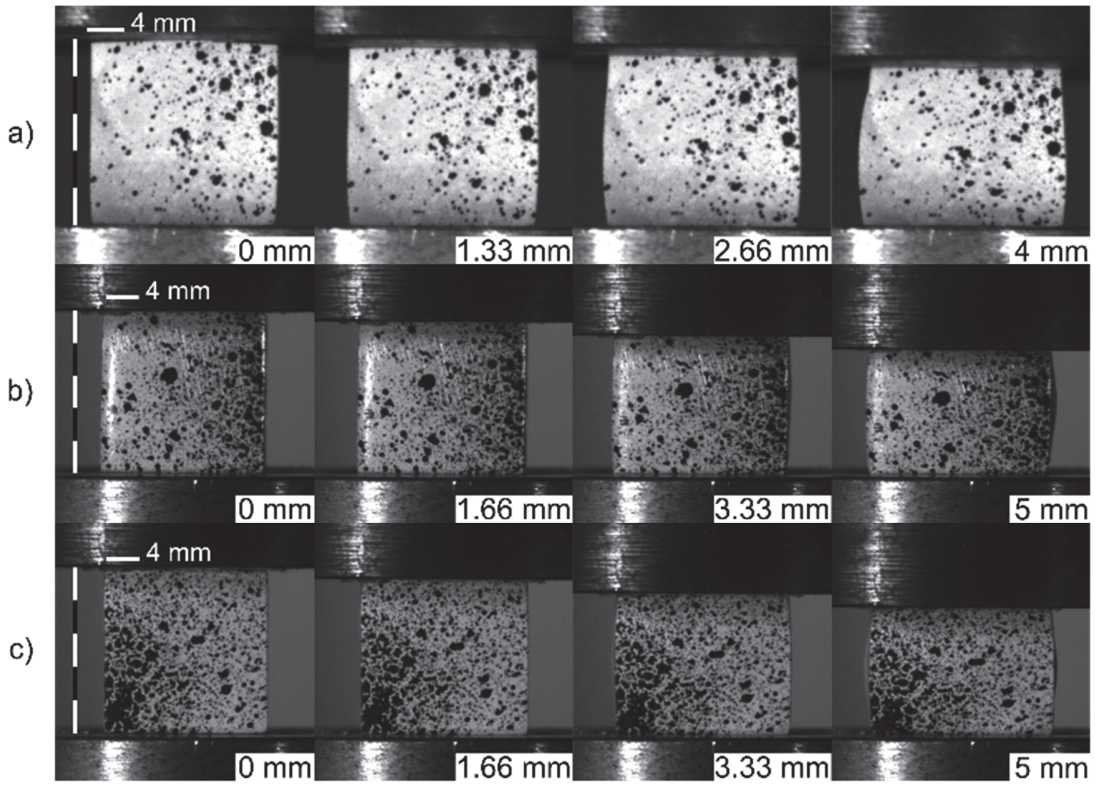

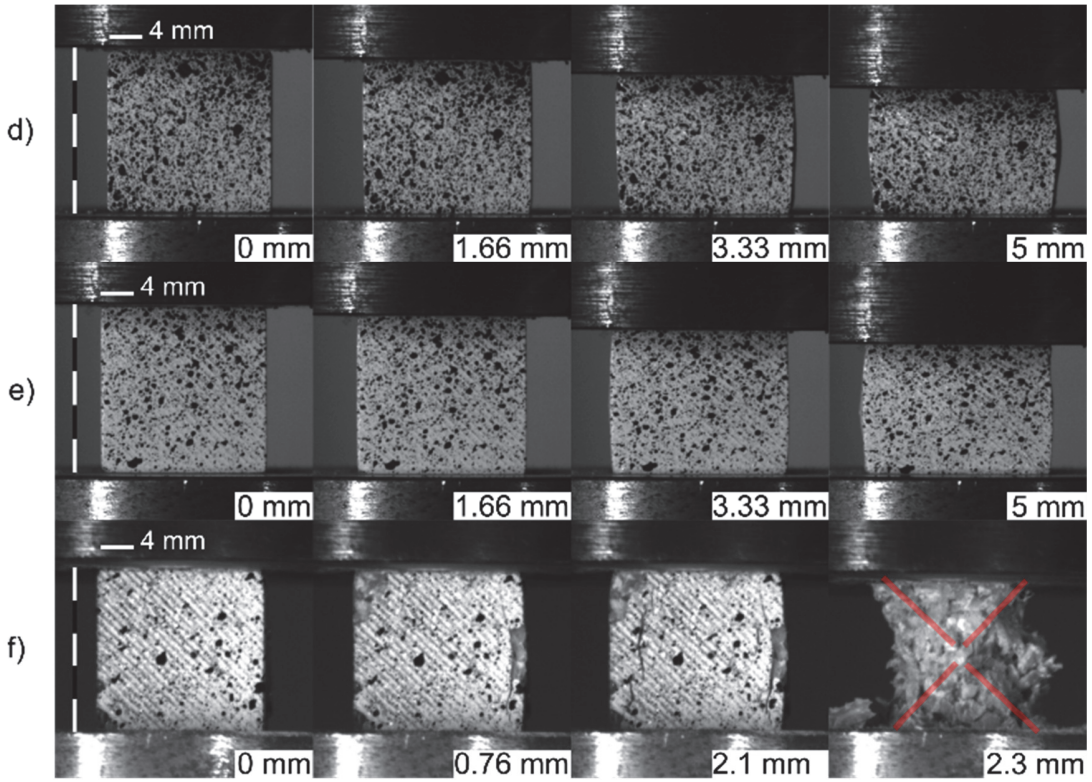

Figure 11: Failure process of molded thermosetting polymers a) crosslinked epoxy resin, b) crosslinked polyester resin, c) crosslinked PUR resin, d) crosslinked PUR resin filled with 100% ATH additive, e) crosslinked PUR resin filled with 200% ATH additive, f) polyester-crushed stone composite with cone shape (highlighted by red lines) as final failure mode (The magnitude of vertical displacements was indicated on figures).

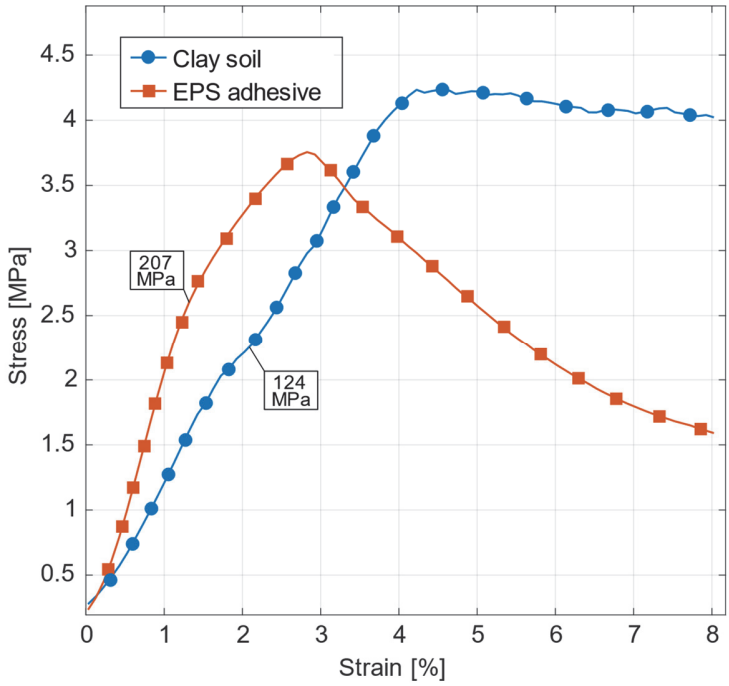

Figure 12: The stress-strain diagram of compression tests of low strength materials (with indicated Young's moduli).

Test results for low-strength materials

Specimens were also made of clay soil and EPS adhesive for compression tests. The stress-strain curves of the compression tests of these materials are shown in Fig. 12. Fig. 13 a) and b) show the phases of compression and the failure of each specimen. Both materials show similar behavior as materials used in building industry (especially to mortar), but much lower strength and stiffness values were obtained.

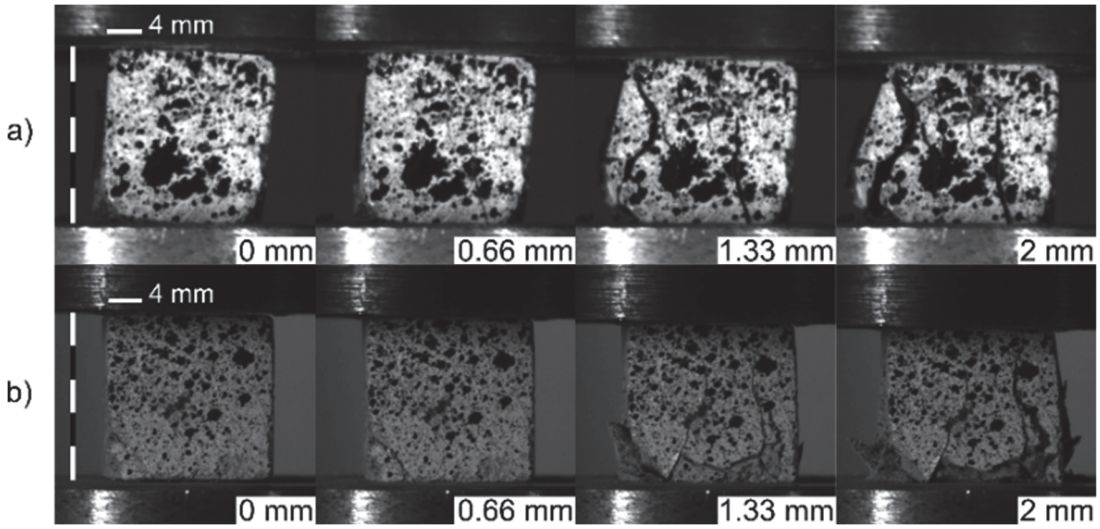

Figure 13: Failure process of low strength materials a) clay soil, b) EPS adhesive (The magnitude of vertical displacements was indicated on figures).

The evaluation of the applied process to produce grain analogs

Of the AM processes, the use of PolyJet and Multi Jet Fusion technology is advised to productively create grains in large quantities, with different or identical geometry. To test the proposed molding process, master grains were printed on top of a plate with FDM technology (Fig. 14 a) which was used the create a silicone mold (Fig. 14 b). Simplified grains were directly printed with PolyJet (Fig. 15 b) and FDM (Fig. 15 c) AM technologies to test the acquired precision. Then, the silicone mold was filled with ceramic powder to produce the artificial grains seen in Fig. 15 a.

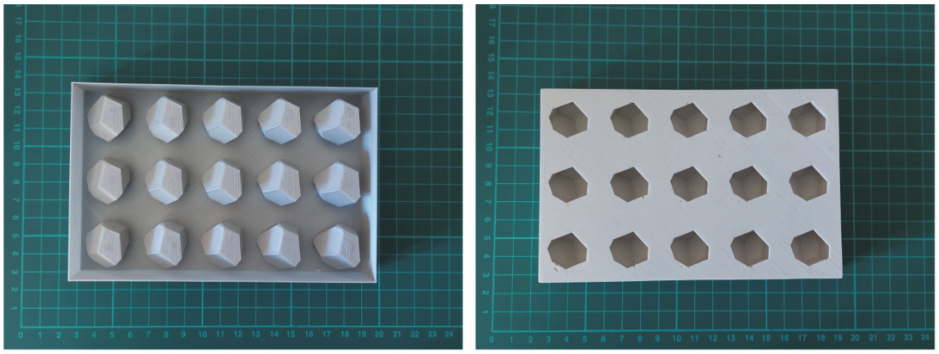

Figure 14: Produce the grain analogs a) additive manufactured master mold with grains, b) silicone mold made with the help of master mold (The grid size is in cm).

Both AM and molded specimens approximate the shape of the irregular grain samples well as shown in Fig. 15, however, the AM technology creates different surface roughness on every side of the specimens. In the case of molded grains, the roughness on the opened surface differed from the other faces of the grains. Furthermore, there is another potential in the AM and moldable technologies, when not only convex but also concave grains can be produced.

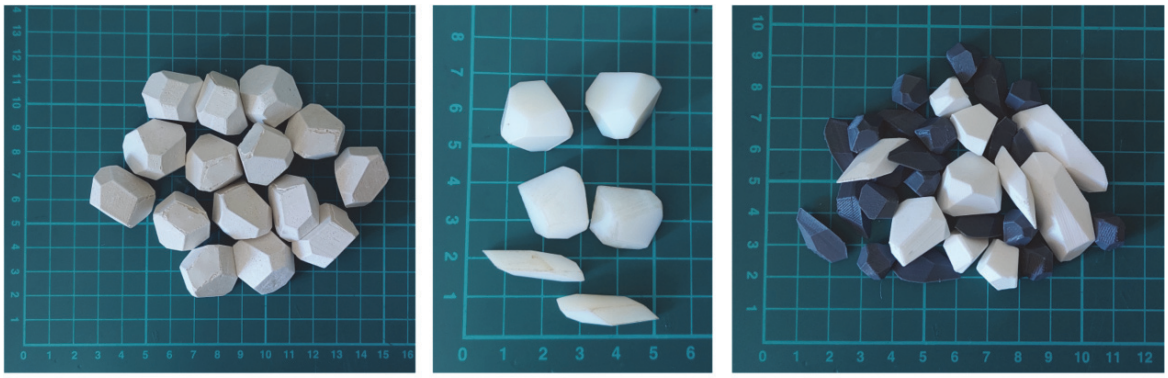

Figure 15: Produced grain analogs a) molded grains of ceramic powder, b) AM grains with PolyJet, c) AM grains with FDM (The grid size is in cm).

The use of ceramic powder is advised of the materials applied in construction industry because they are easily moldable and have a short solidification time. During visual inspection, their surface roughness appeared similar to that of railway ballast grains. Of moldable thermosetting polymers, the polyester-crushed stone composite is recommended due to its relatively high stiffness and strength as well as their failure mode.
In addition, certain materials and technologies may be suitable to model other types of grains and assemblies besides railway ballast. For example, soil, recycled concrete aggregate, agricultural granular materials, fruits, and are considered to be investigable using additively manufactured grains. However, further investigations are required in each case.

Discussion

Tab. 2 shows the compressive strength, the strain at failure and the compressive Young's modulus of each tested specimen. The highest compressive strengths and compressive Young's moduli were measured in the case of railway ballast materials. Of the artificial materials, the crosslinked polyester resin specimens had the highest compressive strength, but the exact values are not known, because the measuring limit of the testing machine was reached. The crosslinked polyester resin specimens developed cracks, but they did not break into several pieces. The second highest compressive strength was measured in the case of the polyester-crushed stone composite. Of the polymer-based specimens, the compressive Young's modulus of the polyester–crushed stone was the closest to the compressive Young's modulus of railway ballast materials, and the final failure mode was also the same in some cases, which was sudden, explosive breakage. This phenomenon was not observed in the case of other studied materials, however, the fracture surface was different than in the case of andesite and basalt.
The strength of the molded, ATH filled PUR polymers increased with increasing filling rate, but on the other hand, the specimens became more prone to breakage.
Specimens produced with PolyJet technology had the second highest compressive strength after the crosslinked polyester resin specimens, however the compressive Young's modulus of this material was not higher than other tested polymers.
Similarly to molded thermosetting polymers, grains from construction materials can be produced with molding. The ceramic powder has the highest Young's modulus out of the studied specimens, but this value is still about half of the basalt's and one-third of the andesite's Young's modulus. The compressive strength values of ceramic powder was the highest between the studied construction materials, but only half the value of the polyester-crushed stone composite, and one-fifth the value of andesite and basalt. Although the ceramic powder is prone to breakage, based on the compression tests, its fracture mode differs from andesite's and basalt's failure.
Bending tests have been carried out on those materials which developed cracks or broke during the compression tests, similarly to the railway ballast materials. Tab. 3 shows the flexural strength, strain at flexural strength and flexural modulus of flexural specimens. The andesite and basalt have the highest flexural strength. Although, the measured flexural strength was higher in the case of crosslinked polyester resin, it is not comparable to the other results, because it has an excessive flexibility compared to the other studied materials, therefore it did not break in several cases. Polyester-crushed stone composite and ceramic powder had the highest flexural strength value after andesite and basalt, but there is no difference

in the order of magnitude. On the other hand, ceramic powder has about twice as high flexural Young's modulus value as polyester-crushed stone, and has a slightly higher flexural Young's modulus value than basalt and andesite.

Material	Compressive strength [MPa]	Strain at failure [%]	Compressive Young's modulus [MPa]
Andesite	207.31	0.78	27,118
Basalt	205.45	0.84	23,835
Socket leveler	24,03	0.95	2732
Concrete	26.96	0.51	6062
Crosslinked epoxy resin	68.66	8.04	1031
EPS adhesive	3.80	2.84	207
FDM ABS 100%[1]	31.40*	6.11*	778
FDM TPLA 100%[1]	40.47*	7.14*	866
FDM PLA 60%[1]	22.22	4.48	663
Mortar	21.27	0.93	2534
Ceramic powder	41.05	0.36	11,870
Crosslinked polyester resin	Out of measuring range	Out of measuring range	1189
Polyester-crushed stone composite	78.30	1.79	4845
PolyJet RGD 835	81.33	9.36	1030
PUR0[2]	22.31	5.37	545
PUR100[2]	26.59*	4.82*	867
PUR200[2]	31.62	5.82	1148
Multi Jet Fusion PA12	40.61**	4.61**	1075
Clay soil	4.55	6.07	124

[1] The percentage indicates the filing of the compression specimen.
[2] The number indicates the quantity of ATH adhesive in percentage.
* Compression stress at yield.
** Stress and elongation measured at 1% residual and elastic deformation.

Table 2: The results of compression tests

Material	Flexural strength [MPa]	Strain at flexural strength [%]	Flexural Young's modulus [MPa]
Andesite	34.33	0.38	8784
Basalt	25.01	0.28	8679
Socket leveler	7.71	0.11	7007
Concrete	6.93	0.09	8320
EPS adhesive	1.85	0.15	1399
Mortar	7.60	0.12	6377
Ceramics powder	18.71	0.18	10,423
Crosslinked polyester resin	57.41*	4.31*	1715
Polyester-crushed stone composite	20.59	0.42	5408

* Limit of bending stress and the associated elongation.

Table 3: The results of bending tests

Conclusion

In this study, several materials and additive manufacturing and molding techniques were investigated to create simplified railway ballast grain analogs.
The following conclusions can be drawn based on the experimental results:

(1) The mechanical behavior of additively manufactured specimens created with PolyJet and Multi Jet Fusion were the closest to andesite and basalt, although they had still considerably lower mechanical properties. Furthermore, they are incapable of breaking.
(2) The material properties of the investigated molded materials are closer to the properties of railway ballast materials than the investigated additive manufactured materials. Of the moldable materials, the ceramic powder and polyester resin mixed with fine-graded crushed stone had the most suitable mechanical and failure properties.
(3) The molding process that uses silicone molds can be utilized to produce high-strength compared to additive manufacturing technologies, artificial grains at lower cost.
(4) The additive manufacturing and molding technologies can be used to create replicable, artificial, simplified railway ballast grains that can be used in future experimental shape-effect studies.
(5) In the case of building an assembly in which the grains are mostly different, they shall be created directly with additive manufacturing techniques.
(6) The utilization of molding techniques are recommended when numerous grains with identical shape need to be produced efficiently. It should be mentioned that for the creation of molds, additively manufactured grains are still necessary to create the final shape of the mold.

Since the range of the material of test specimens was limited, further studies will be needed to investigate additional materials, which can be used to produce grains with arbitrary shape.

ACKNOWLEDGEMENT

The authors are grateful for the inspiration of this research topic to Professor Katalin Bagi. The help of the personnel at the BME Department of Machine and Product Design, the BME Department of Polymer Technology and the Industrial Service Center Kft. in manufacturing the specimen and conducting the tests is gratefully acknowledged.
The research reported in this paper and carried out at BME has been supported by the NRDI Fund (TKP2020 NC, Grant No. BME-NCS) based on the charter of bolster issued by the NRDI Office under the auspices of the Ministry for Innovation and Technology.
The research has been partially supported by the NKFI OTKA K-138642 grant of the Hungarian Ministry for Innovation and Technology.

REFERENCES

[1] Juhasz, E., Fischer, S. (2019). Specific Evaluation Methodology of Railway Ballast Particles' Degradation, Sci. Transp. Progress. Bull. Dnipropetr. Natl. Univ. Railw. Transp., 0(3(81)), pp. 96–109, DOI: 10.15802/stp2019/171778.
[2] Bai, H., Du, W., Shou, Y., Chen, L., Berto, F. (2021). Experimental investigation of cracking behaviors of ductile and brittle rock-like materials, Frat. Ed Integrita Strutt., 15(56), pp. 16–45, DOI: 10.3221/IGF-ESIS.56.02.
[3] Rad, M.M., Safikhani, S., Bauer, E. (2019). Influence of the loading condition on single grain crushing in DEM simulation, Period. Polytech. Civ. Eng., 63(4), pp. 1152–1158, DOI: 10.3311/PPci.14541.
[4] Ma, H., Zhao, Y. (2018). Investigating the flow of rod-like particles in a horizontal rotating drum using DEM simulation, Granul. Matter, 20(3), pp. 1–15, DOI: 10.1007/s10035-018-0823-0.
[5] Kodam, M., Bharadwaj, R., Curtis, J., Hancock, B., Wassgren, C. (2010). Cylindrical object contact detection for use in discrete element method simulations, Part II-Experimental validation, Chem. Eng. Sci., 65(22), pp. 5863–7581, DOI: 10.1016/j.ces.2010.08.007.
[6] Maione, R., Kiesgen De Richter, S., Mauviel, G., Wild, G. (2017). Axial segregation of a binary mixture in a rotating tumbler with non-spherical particles: Experiments and DEM model validation, Powder Technol., 306, pp. 120–129, DOI: 10.1016/j.powtec.2016.10.073.
[7] Härtl, J., Ooi, J.Y. (2008). Experiments and simulations of direct shear tests: Porosity, contact friction and bulk friction, Granul. Matter, 10(4), pp. 263–271, DOI: 10.1007/s10035-008-0085-3.
[8] Wu, Y., Yamamoto, H., Izumi, A. (2016). Experimental investigation on crushing of granular material in one-dimensional test, Period. Polytech. Civ. Eng., 60(1), pp. 27–36, DOI: 10.3311/PPci.8028.
[9] Zhao, B., An, X., Wang, Y., Zhao, H., Shen, L., Sun, X., Zou, R. (2020). Packing of different shaped tetrahedral particles: DEM simulation and experimental study, Powder Technol., 360, pp. 21–32, DOI: 10.1016/j.powtec.2019.09.072.

[10] Miskin, M.Z., Jaeger, H.M. (2013). Adapting granular materials through artificial evolution, Nat. Mater., 12(4), pp. 326–331, DOI: 10.1038/nmat3543.
[11] Athanassiadis, A.G., Miskin, M.Z., Kaplan, P., Rodenberg, N., Lee, S.H., Merritt, J., Brown, E., Amend, J., Lipson, H., Jaeger, H.M. (2014). Particle shape effects on the stress response of granular packings, Soft Matter, 10(1), pp. 48–59, DOI: 10.1039/c3sm52047a.
[12] Landauer, J., Kuhn, M., Nasato, D.S., Foerst, P., Briesen, H. (2020). Particle shape matters – Using 3D printed particles to investigate fundamental particle and packing properties, Powder Technol., 361, pp. 711–718, DOI: 10.1016/j.powtec.2019.11.051.
[13] Hanaor, D.A.H., Gan, Y., Revay, M., Airey, D.W., Einav, I. (2016). 3D printable geomaterials, Geotechnique, 66(4), pp. 323–332, DOI: 10.1680/jgeot.15.P.034.
[14] Li, Y., Zhou, H., Liu, H., Ding, X., Zhang, W. (2021). Geotechnical properties of 3D-printed transparent granular soil, Acta Geotech., 16(6), pp. 1789–1800, DOI: 10.1007/s11440-020-01111-7.
[15] Adamidis, O., Alber, S., Anastasopoulos, I. (2020). Assessment of three-dimensional printing of granular media for geotechnical applications, Geotech. Test. J., 43(3), pp. 641–659, DOI: 10.1520/GTJ20180259.
[16] Ahmed, S.S., Martinez, A. (2020). Modeling the mechanical behavior of coarse-grained soil using additive manufactured particle analogs, Acta Geotech., 15(10), pp. 2829–2847, DOI: 10.1007/s11440-020-01007-6.
[17] Kittu, A., Watters, M., Cavarretta, I., Bernhardt-Barry, M.L. (2019). Characterization of additive manufactured particles for DEM validation studies, Granul. Matter, 21(3), pp. 1–15, DOI: 10.1007/s10035-019-0908-4.
[18] DIN 53453:1975-05, Testing of Plastics; Impact Flexural Test.
[19] ISO - ISO 604:2002 - Plastics — Determination of compressive properties. Available at: https://www.iso.org/standard/31261.html. [accessed August 2, 2021].
[20] ISO - ISO 178:2019 - Plastics — Determination of flexural properties. Available at: https://www.iso.org/standard/70513.html. [accessed August 2, 2021].
[21] Sgambitterra, E., Niccoli, F. (2021). Inverse problems with the digital image correlation: approach and applications, Frat. Ed Integrità Strutt., 15(57), pp. 300–20, DOI: 10.3221/igf-esis.57.22.
[22] Yang, D., Wang, X. (2019). Damage evolution law on the surface field of argillaceous dolomite based on Brazilian test and 3D digital image correlation, Frat. Ed Integrita Strutt., 13(48), pp. 144–51, DOI: 10.3221/IGF-ESIS.48.17.
[23] Suhr, B., Six, K. (2017). Parametrisation of a DEM model for railway ballast under different load cases, 19, pp. 64, DOI: 10.1007/s10035-017-0740-7.
[24] Fischer, S. (2021). Investigation of effect of water content on railway granular supplementary layers Reinforcement of railway substructure (embankment) with special materials View project Optimisation of life-cycle costs of tramway superstructures View project INVESTIGATION, (3), DOI: 10.33271/nvngu/2021-3/064.